A Scaled, Performance Driven Evaluation of the Layered Sensing Framework Utilizing Polarimetric Infrared Imagery

Hamilton Scott Clouse[a] and Hamid Krim[a] and Olga Mendoza-Schrock[b]

[a]North Carolina State University, Campus Box 7911, Raleigh, North Carolina;
[b]Air Force Research Laboratory, 2241 Avionics Circle, Wright-Patterson AFB, Ohio

ABSTRACT

The layered sensing framework, in application, provides a useful, but complex integration of information sources, e.g. multiple sensing modalities and operating conditions. It is the implied trade-off between sensor fidelity and system complexity that we address here. Abstractly, each sensor/source of information in a layered sensing application can be viewed as a node in the network of constituent sensors. Regardless of the sensing modality, location, scope, etc. each sensor collects information locally to be utilized by the system as a whole for further exploitation. Consequently, the information may be distributed throughout the network and not necessarily coalesced in a central node/location. We present, initially, an analysis of polarimetric infrared data as one of the input modalities to such a system. We then proceed with statistical and geometric analyses of an example network, thus quantifying the advantages and drawbacks of a specific application of the layered sensing framework.

Keywords: layered sensing, distributed sensing, polarimetric, infrared, tracking, feature-aided, fusion, multi-sensor

1. INTRODUCTION

Information is everywhere and in many different forms. Even electronic information is available in vast amounts and is generated by a plethora of sensors and sources. In terms of decision making, especially, more information is always better, but how does one cope with the inevitable inundation? Classically, the integration of such abundant information has required many individuals, specialized in their particular process or data-type, working in tandem to analyze all of the individual data streams and then report to a single individual or group who will perform further analysis, on the whole, to draw conclusions and act accordingly. Now, with the immense stores of data at our disposal and the need for real-time decision making becoming more critical, we can no longer supply the manpower nor the time to perform analysis in the classical way. One idea proposed to combat this impending juggernaut is layered sensing.

Defined in [1], layered sensing is a framework for aggregating and presenting information. As the name implies, the framework assumes multiple "sensors," or information sources, as input. The result of the utilization of the framework is an aggregated presentation for use by individuals/groups to improve their understanding of the scenario under observation. Furthermore, as it has been proposed by the Layered Sensing Leadership Group (LSLG) at the Air Force Research Laboratory (AFRL), the focus of the employment of such a tool is termed "situational awareness," whereby decision makers are made privy to a wealth of information germane to a scenario in a coherent fashion that would otherwise be unavailable. The novelty and utility of such a framework is clear when one considers the plethora of information sources at hand, e.g.: video, vibration sensors, satellite photography and processes such as object tracking, speech recognition and behavior analysis. A look at the implications and challenges of this framework can be found in [2].

Simplistically, layered sensing is the idea that all of the data pertinent to a chosen goal can be amalgamated automatically into a kind of omniscient data oracle, thus enabling better informed decision making in a timely

Further author information: (Send correspondence to H.C.)
H.C: E-mail: hsclouse@ieee.org
A.K.: E-mail: ahk@ncsu.edu
O.M.: E-mail: olga.mendoza-schrock@wpafb.af.mil

manner. The output of the layered sensing framework, when applied to a particular goal, would enhance the decision-makers' knowledge of the scenario by providing a coherent presentation of the whole relevant data; it is such an integration and the advantages thereof that we consider.

A key tenet of layered sensing is the integration of the different data sources with one goal (application) in mind. Here we explore such an integration by observing a single scene through two different sensing modalities with the goal of tracking an object moving through the scene. We evaluate a standard feature-aided tracker for each modality independently, for both together (via decision-level fusion), and then for both together with decreased resolution on the part of each sensor, to evaluate some claims about layered sensing:

- Higher accuracy is attainable by combining multiple data sources.
- The accuracy achieved with each independent modality tracker is attainable with the combined tracker utilizing lower fidelity data from each independent modality.
- The combined tracker will continue to function in the case of the loss of one sensor input.

Our approach draws inspiration from biological organization wherein particular agents perform specific tasks and the whole society of agents benefits from each; thus our work is influenced by parallel/distributed computation ideas. We abstract the sensors and their data as nodes in a network structure through which the information is shared. Following this line of thought, we will first evaluate a particular data type, polarimetric infrared video, in a geometric fashion to derive appropriate features for use as input to a standard tracking algorithm, then we'll proceed to construct the combined tracker, utilizing this data set and another. The evaluation process will be performed on the resulting tracking outputs. Finally we'll look at the computational complexity of the trackers to compare the possible trade-offs in accuracy.

The organization of the rest of the paper is as follows: Sect.2-Background, Sect.3-Data Description, Sect.4-Methods, Sect.5-Results, and Sect.6-Conclusions.

2. BACKGROUND

There are a couple topics discussed in this paper for which we will now briefly proceed to establish some understanding: the nature of polarized electromagnetic (EM) radiation and the implications and inferences associated with the infrared (IR) band of the EM spectrum.

2.1 Polarization of EM Radiation

To begin with, let's draw from our intuition about visible light. When, on a sunny day, one views a window on an automobile, reflected rays from the sun can cause a glare, thus hindering vision. One means of combating this is donning sunglasses with polarized lenses. These lenses, along with the tinting to reduce the intensity of the light transmitted to the eyes, also act as vertically polarizing filters. The reflected light that causes the glare is, generally, horizontally polarized due to the orientation of the window. The vertical polarizing filters only transmit light that is also vertically polarized and therefore the glare is prevented.

Another example of the use of polarizing filters is in the presentation of 3-D movies. Linear polarizers have been used in the necessary viewing glasses since the late 1930's. More recently circular polarizers have been implemented (a little more difficult to intuit) in such theater glasses. These technologies produce stereoscopic 3D images by creating the illusion of depth perception. A polarizing filter is placed over each eye, one oriented orthogonally to the other, such that each eye observes a different image.

There is much history, mostly from the field of physics (see Ref.'s 3, 4,and 5), behind the understanding and exploration of polarization of EM waves, in general. Here, we will skip straight to the utilization of the formalism that well describes the phenomenon.

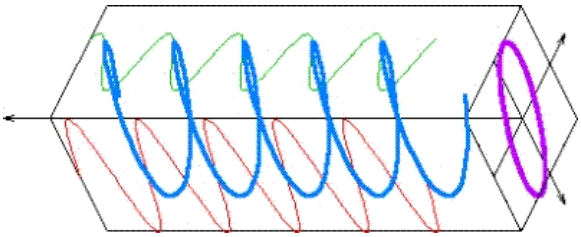

Figure 1. In general, the E-field component of an EM wave rotates about the transverse axis and thus traces an ellipse in the plane of rotation and can be decomposed into orthogonal components E_{0_X} and E_{0_Y}.

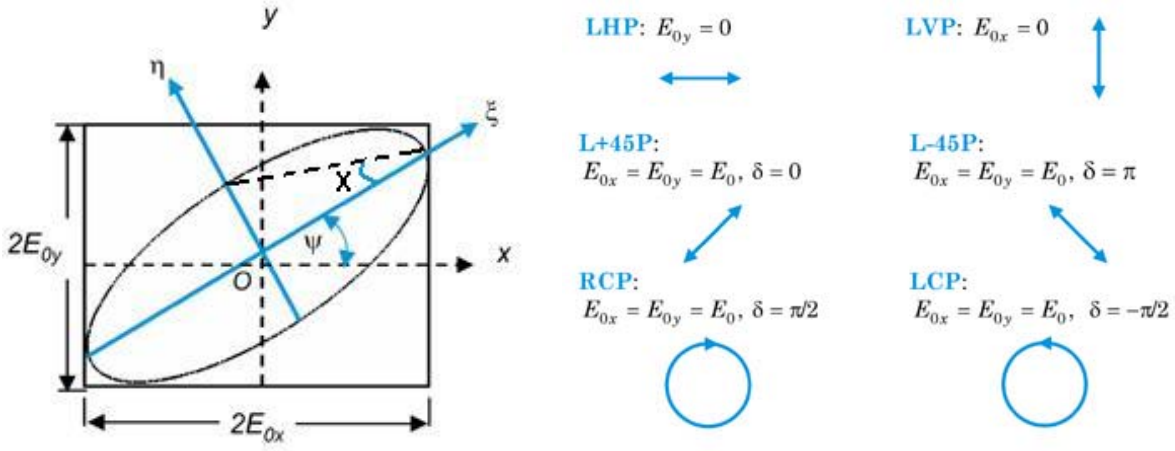

(a) (b)

Figure 2. The polarization ellipse (a) with the labelled parameters and the degenerate states it can take (b). From [6]

2.1.1 Mathematical Analysis

The electric wave, as it propagates will, in general, have some rotation about the z-axis and will thus trace out an ellipse in the plane of rotation, as shown in Fig.1. The ellipse that is traced out can be described via the properties of the electric wave as indicated in Fig.2a.

Of course, for different values of E_{0_X}, E_{0_Y}, and δ (the phase difference between the two orthogonal waves) the ellipse will have different shapes. There are certain states, called degenerate states, that are produced for certain values of interest for these parameters, that act as a basis by which any generally polarized waveform can be described completely (Fig.2b). That is exactly what the Stokes' vector representation exploits.

2.1.2 Stokes' Vector Relations

Sir George Gabirel Stokes, in 1852, wrote a paper[7] in which he proposed a convenient means to describe incoherent polarized light in the form of vector (or a set of parameters), S. This idea was novel particularly for the interpretation of each parameter as a measure of the "preference" of the observed light toward a certain direction of polarization. The vector is a set of four elements:

- S_0 - intensity
- S_1 - horizontal preference
- S_2 - $+45^o$ preference
- S_3 - right circular preference

In this formalism the intensity parameter S_0 is, for example in imaging, the picture one would normally capture with a camera. The preference images (parameters, elements, etc.) are relations between pairs of degenerate states representing the observed light, e.g. the horizontal preference (S_1) is the difference in intensities of the horizontal (LHP) and vertical (LVP) degenerate states that characterize the observed light.

Another advantage of the Stokes' vector formalism is the ease of calculation from readily measurable phenomena. By observing light through a linear polarizing filter and a waveguide of thickness $\frac{\lambda}{4}$, where λ is the wavelength of the observed light, at various orientations one can observe the representative degenerate states (Fig.2b), from which the Stokes' vector can be determined.

The following equation relates the Stokes' vector representation (S) to the collected image representation (I_ϕ) and also to the orthogonal linear (X,Y) basis (where δ is the phase difference as in Fig.2):

$$S = \begin{bmatrix} S_0 \\ S_1 \\ S_2 \\ S_3 \end{bmatrix} = \begin{bmatrix} a^2 \\ a^2 cos(2\chi)cos(2\psi) \\ a^2 cos(2\chi)sin(2\psi) \\ a^2 sin(2\chi) \end{bmatrix} = \begin{bmatrix} E_{0_X}^2 + E_{0_Y}^2 \\ E_{0_X}^2 - E_{0_Y}^2 \\ 2E_{0_X}E_{0_Y}cos(\delta) \\ 2E_{0_X}E_{0_Y}sin(\delta) \end{bmatrix} = \begin{bmatrix} \frac{1}{2}\left(I_0 + I_{45} + I_{90} + I_{135}\right) \\ I_0 - I_{90} \\ I_{45} - I_{135} \\ I_R - I_L \end{bmatrix} \tag{1}$$

In the above equation, ψ is the angle of polarization (AoP), χ is the angle of ellipticity (see Fig.2a), a is the radiant intensity, and the I_ϕ's are the images collected through a linear polarizing filter with orientation ϕ-degrees counter-clockwise from horizontal.

2.1.3 Intensity Invariants from Polarization Information

There are two key images that can be derived from the Stokes' vector representation of polarization data: the Degree of Linear Polarization (DoLP) and the Angle of Polarization (AoP). The DoLP is a ratio of the lengths of the minor and major axes of the polarization ellipse: $|cos(2\chi)|$ where $|\cdot|$ represents the absolute value operator. The AoP is the orientation of the major axis of the polarization ellipse, ψ. These images, as can be deduced from the formulae in Eqn.'s 2 and 3, are invariant to intensity (a from Eqn.1), and are therefore physically influenced geometric features not attainable from traditional imaging techniques, i.e. imaging without a waveguide and polarizing filter.

$$DoLP = \frac{\sqrt{S_1^2 + S_2^2}}{S_0} = |cos(2\chi)| \tag{2}$$

$$AoP = \psi = \frac{1}{2}tan^{-1}\left(\frac{S_2}{S_1}\right) \tag{3}$$

2.2 Infrared Band Implications

In Sect.2.1 our discussion did not focus on any specific band of the EM spectrum, though some intuition from visible light was called upon in the given examples. The formalism is indeed applicable to all frequency ranges of the EM spectrum. In remote sensing, diversity among modalities is a necessity and here we focus on an imaging type that caters to such a requirement. Imaging in the infrared band is useful for observation in low-light conditions as IR sensors, while working in a relatively small band and collecting relatively few photons, are very accurate and thus, with proper scaling, allow for object discernment under a greater range of operating conditions than does visible light imaging.[8]

Within the infrared band ($\lambda \in [0.7, 14]\mu m$) there are several sub-bands defined:

1. near infrared (NIR) for ($\lambda \in [0.7, 1]\mu m$)
2. short-wave infrared (SWIR) for ($\lambda \in [1, 3]\mu m$)
3. mid-wave infrared (MWIR) for ($\lambda \in [3, 5]\mu m$)
4. long-wave infrared (LWIR) for ($\lambda \in [8, 14]\mu m$)

These different bands are defined by the bandwidth that different sensor types cover, e.g. NIR is from the end of perception by the human eye through the response of silicon based detectors.[9] Our work focuses on the band LWIR. As can be seen in Fig.3, reflections dominate all the IR bands, as in the visible light spectrum, except for the LWIR band. In the LWIR band emitted radiation is dominant, i.e. thermal emissions. The advantage of imaging in this band is that heat/radiation sources themselves are observed and small sources are not so obstructed by the reflections/shadows from larger/stronger sources, e.g. the sun, as they would be in other bands. While this may cause some problems, e.g. there are multiple sources instead of one strong one (e.g. the sun), it simplifies many calculations since the need to take into account reflections and shadows is not as great when concerned with moving objects in a scene. This is not to say that shadows and reflections do not occur, but simply that because heat transfer is a relatively slow process compared with visible light transmittance, and even video capture rates, they are negligible over short time intervals.

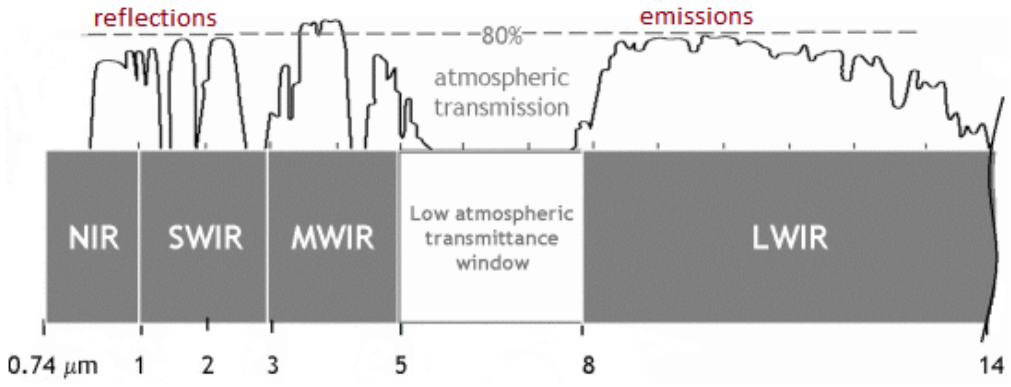

Figure 3. The Infrared band of the EM spectrum with radiance curves for reflections and thermal emissions. Clearly emissions dominate the spectrum in the LWIR. From `http://mivim.gel.ulaval.ca` accessed August 30, 2010.

3. DATA DESCRIPTION

Since the goal of this work was an initial evaluation of some of the claims about the layered sensing framework, the data sets utilized were similar to facilitate performance evaluations. The two data sets were both video of the same scene and both captured in the LWIR band. The first data type is standard LWIR (thermal) video and the second is also LWIR video, but polarized via linear polarizing filters. This second data set is termed polarimetric IR (PolarIR). Even though the data sets are very similar, the difference in the feature sets derived from each is sufficient for evaluating them as different data sources. The same camera was used to collect both data sets to ensure that the diversity between the data sets was due to the different modalities and not physical differences in the equipment, calibrations, etc..

Each video was captured with a 480×640 element focal-plane array (FPA) such that each frame is a 2×2 array of the four polarizer orientations (i.e. each polarization image is 240×320). The scene observed is composed of a series of intersecting streets with one intersection as the focus. In the scene there are several parked automobiles, trees, and street lamps. The portion of the scene utilized for our analysis captures only one moving object, an automobile traveling along one of the roads. An example image from the data set, with the moving automobile visible, is shown in Fig.4.

3.1 Infrared (IR)

The collection and utilization of thermal imagery/video is common in remote/passive sensing applications. In this data type the brightness of the pixels in the image are measures (integration over exposure time) of the emitted radiance of the objects in the scene, i.e. thermal signatures. This thermal diversity within a scene promotes the utilization of segmentation and tracking techniques common to electro-optical (visible light band) imagery/video.

Figure 4. A cleaned sample image from the scenario observed for this work. Notice the parked cars along the street and the truck in the foreground travelling along the road. This truck was the focus of our tracking effort.

3.2 Polarimetric Infrared (PolarIR)

The PolarIR, the modality of the second data type, quantizes the polarization diversity of the emitted radiation observed. This data is collected, as stated earlier, through the use of linear polarizing filters to collect the I_ϕ's, as referenced in Sect.2.1.2. This information lends itself toward the development of feature sets more directly influenced by the geometry of the scene, e.g. the angle of polarization, as described in Sect.2.1.3.

For this particular data set, several different geometric features were available for exploitation. Along with the invariants listed in Sect.2.1.3, other properties of the observed electric wave were considered. Two, in particular, proved to be more descriptive for our tracking problem. The first was similar in derivation to the DoLP (Eqn.2), but includes the sign of the $cos(2\chi)$ function:

$$\rho = cos(2\chi) = \frac{S_2}{S_0 \cdot sin(2\psi)}. \tag{4}$$

The second feature is more closely related to the wave description of the observed intensities, namely δ, the phase difference discussed in Sect.2.1.1.

$$\delta = cos^{-1}\left(\frac{S_2}{\sqrt{S_0 + S_1}\sqrt{S_0 - S_1}}\right). \tag{5}$$

Example output images from these two features can be seen in Fig.5.

These are both discriminating features for this modality with many desirable geometric properties, but for this work we only utilized the δ feature as input for our tracking algorithm. Our current plans for future work include implementation of both of these features as well as some other geometric/physical relationships available from this data type.

4. METHODS

The tracking portion of this work relied on a standard technique, the use of a Kalman filter. To further simplify the procedure, the centroid of the truck moving through the scene was the point being tracked. As described in [10], the Kalman filter was implemented with four state variables: one each for the row and column positions and the associated velocities. The filter was initialized with the centroid being located in the center of the frame and having no velocity. The observation for each update was taken to be the centroid of the largest moving object located within the area predicted by the filter.

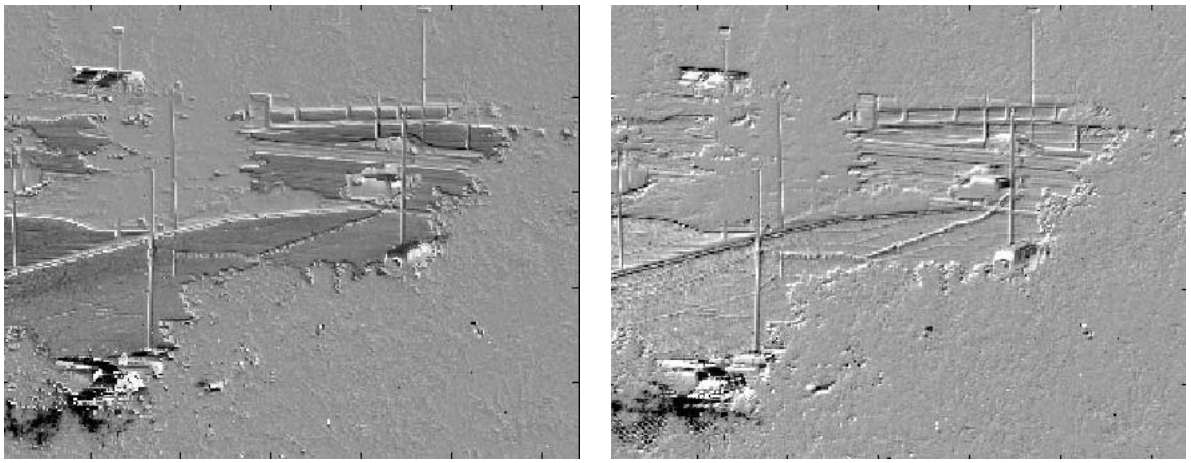

(a) (b)

Figure 5. Example images produced by the new features ρ(a) and δ(b).

4.1 Tracker Performance

To determine the performance characteristics of the applications of the tracking algorithm, mainly the accuracy, ground truth information for the data was required. Instead of relying on other automatic techniques to provide the true locations of the truck in each frame, the truck was tracked manually. That is, an individual determined the location of the truck in each frame and a set of simple morphological operations were utilized to calculate the centroid of the truck. This method of "truthing" the data ensures that not only is the information accurate, as a person would perceive it, but errors and faults of other automatic tracking algorithms do not interfere with the performance analysis of those in question.

Once the tracking algorithms had been run, the results were compared to the truth data and the Euclidean distance (in the image plane) from the true centroid location of the truck to that predicted by the tracker was calculated. The average deviation (Eqn.6) for each tracker was calculated over the whole scene. This measure is what was ultimately used to evaluate the trackers' performance.

$$Err = E\left[\sqrt{(\hat{\theta_r} - \theta_r)^2 + (\hat{\theta_c} - \theta_c)^2}\right] \tag{6}$$

In Eqn.6, $\hat{\theta}$ is the vector of estimated centroid locations from the tracker, θ is the vector of the true centroid locations, $E[\cdot]$ is the expectation operator, and c and r represent the column and row coordinates (in the image plane) of the centroid, respectively.

Also, to further evaluate the trackers, the algorithms were run on the same data sets at different resolutions. After each iteration of the trackers, the resolution of the data was decreased, via two-dimensional down-sampling, and the trackers were run again. This test was performed for a range of downsampling scales to allow for proper interpretation of the trackers' performance.

4.2 Track Fusion

There are many different means to combine, or fuse, data from different sources in to a single representation. The means, methods, and motivations for such techniques are a field of study on their own. The particular form that we focus on in this work is decision-level fusion. Put simply, we combine the results of processes instead of combining the features or the pixel values directly, as one might do with feature-level or pixel-level data fusion. This decision-level fusion meshes nicely with our network abstraction mentioned earlier. Further discussion of these techniques can be found in references [11], [12], [13], and [14].

At a single node in our network we have a sensor, its generated data, and for this particular effort, the tracks from the applied Kalman filter. To maintain the distributed nature of the framework, each node can

only communicate to the neighboring nodes and no single node aggregates all the information from the other nodes. However, since we are currently only working with two nodes, the IR and PolarIR, our network is greatly simplified.

As a result of the use of the Kalman Filter method, we have additional information available, at each node, for every step in the tracking process. Namely, the prediction error covariance matrix is of use. Since each independent tracker calculates the prediction error covariance matrix, P, we can use these values to calculate a confidence measure (Eqn.7) for each tracking result.

$$c = tr\,(PC) \tag{7}$$

In Eqn.7, $C = (c_{ij})$, $i, j \in [1, n]$, $c_{ij} = 0$ for $i \neq j$ and $c_{ii} = 1$ for $i \in [1, k]$ where n is the number of state variables in the tracker, k is the number of state variables to consider in the confidence calculation and $tr(\cdot)$ is the matrix trace function. In our case, k=2 since we're only concerning ourselves with the accuracy of the centroid position estimate.

Therefore, our decision-level fused tracker is simply a decision rule (Eqn.8), evaluated at each node. We use $\hat{\theta}$ to represent the estimate with the subscript 0 indicating the current node and m indicating all of the neighboring nodes.

$$\hat{\theta_0} = \begin{cases} \hat{\theta_m} & \text{if } c_0 > c_m \\ \hat{\theta_0} & \text{else} \end{cases} \tag{8}$$

The nodes calculate a confidence value for their resultant position estimate and compare that value to those of the neighboring nodes. If a neighboring node has a better (smaller) confidence value than the current node, the current node changes its estimate to match that of the neighboring node. Thus, the result of the fused tracker is a consensus among the different independent trackers' outputs.

5. RESULTS

5.1 Accuracy Comparison

As described in Sect.4.1, the performance of each tracker was described as the average deviation for the tracking duration and this calculation was performed for several different frame resolutions, and therefore several different number of pixels on target (P.O.T.). Figure 6 indicates the errors calculated for each tracker as a function of the number of pixels on the target being tracked.

For $10 - 100\%$ of the original number of P.O.T., the fused tracker consistently performs better than the two constituent trackers alone. Particularly for lower P.O.T. values ($10 - 20\%$), the fused tracker offers great advantages in accuracy with as much as a 40% decrease in location prediction error.

5.2 Complexity Analysis

The complexity of the trackers in this work are all the same. Since only a standard implementation of the Kalman Filter method was used, the complexity of the individual trackers is $O(n^3)$. Furthermore, since the fused tracker (the combined tracker) utilized a distributed/parallel structure, its computational complexity is also $O(n^3)$.

6. CONCLUSIONS

With the results shown in the previous section, the claims listed in the introduction certainly seem substantiated, at least in this particular set of experiments. Indeed the fused tracker achieves a higher accuracy, as seen from the lower error rate, than the individual trackers alone indicating that the use of multiple data sources can improve the overall performance. Consequently, the fused tracker with lower fidelity input performed equally as well as the separate trackers with higher fidelity input, thus supporting the second claim. Furthermore, the non-linear nature of the fused tracker presented here becomes evident at lower resolutions of the input data in that it almost maintains its linear trend in error rate while the separate trackers' error rates increase exponentially.

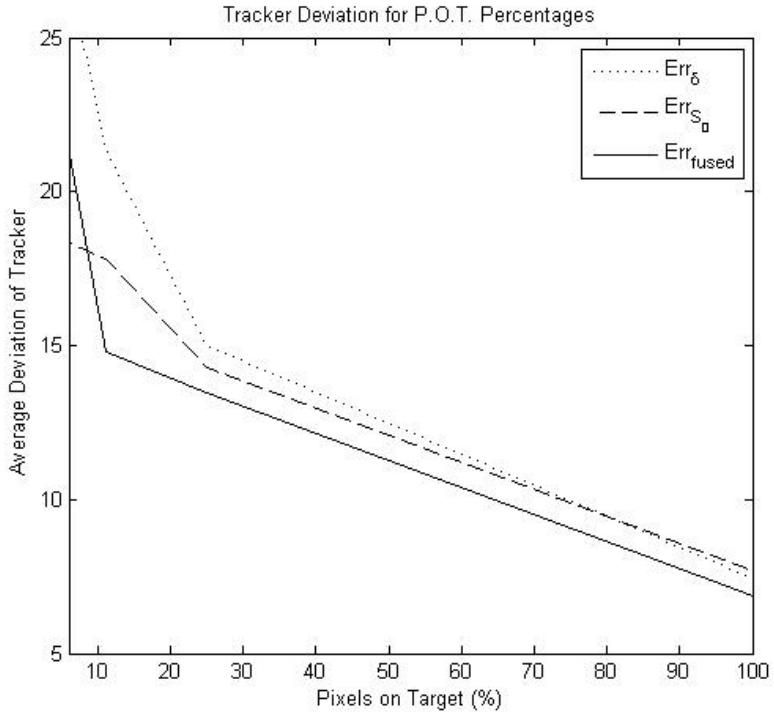

Figure 6. This plot indicates the errors associated with each tracker as a function of the number of pixels on target (as a percentage of the number in the original data set resolution). Here subscripts indicate which tracker error is represented.

As for the third claim, that the fused-tracker will still function in the event of the loss of one of the data inputs, this is addressed more completely in a theoretical fashion. The design of the fused-tracker presented here makes its decisions as a consensus of a network of inputs. If one of the inputs were to be lost, it would not contribute to the consensus and the remaining sources would decide the tracker output. So, for a complete loss of one source, the fused-tracker will still function. In fact, it will do so as long as it has one valid data source. In the event that the data sources become corrupted, but not lost, the Kalman Filter mechanics account for this in the calculation of the prediction error covariance matrix, P. Since the confidence values are directly calculated from these matrices, this fused-tracker is robust to large perturbations in some of the data sources.

Also, due to the parallel nature of the fused-tracker's design, the computational complexity is not altered from that of a standard Kalman Filter implementation of $O(n^3)$, further solidifying the idea that the layered sensing framework is not only a viable means to deal with large amounts of data, but offers additional benefits of accuracy and robustness while not increasing the cost of running the algorithm.

Granted this is an initial test with specific and similar data sets, we plan to continue this work by expanding from tracking in video to pattern recognition in other signal types and other applications. The layered sensing framework, so far, seems to meet a staying and ever-growing need, and does so well.

ACKNOWLEDGMENTS

The authors would like to thank Dr. Ed Watson, Mr. Bob Mack, Dr. Dan Lemaster, and Mr. Ed Zelnio of the AFRL/Sensors Directorate for their assistance, support, and guidance of this work. They would also like to thank Dr. Jon Sjogren for his continued support of the effort. (This document is approved for public release via 88 ABW ???).

REFERENCES

[1] Bryant, M., Johnson, P., Kent, B. M., Nowak, M., and Rogers, S., "Layered sensing: Its definition, attributes, and guiding principles for AFRL strategic technology decelopment," tech. rep., Sensors Directorate, Air Force Research Laboratory (2008).

[2] Wicks, M. C. and Moore, W., "Distributed and layered sensing," in [*International Waveform Diversity and Design Conference*], 233–239 (2007).

[3] Brosseau, C., [*Fundamentals of Polarized Light: A Statistical Optics Approach*], John Wiley & Sons, Inc. (1998).

[4] Goldstein, D., [*Polarized Light*], Marcel Dekker, Inc., 2nd ed. (2003).

[5] Sandus, O., "A review of emission polarization," *Applied Optics* **4**, 1634–1642 (December 1965).

[6] Collett, E., [*Field Guide to Polarization*], SPIE Press (2005).

[7] Stokes, G. G., "On the composition and resolution of streams of polarized light from different sources," *Transactions of the Cambridge Philosophical Society* **9**, 399–416 (1852).

[8] Rogne, T., Stewart, S., and Metzler, M., "Infrared polarimetry: What, why, how, and the way ahead," tech. rep., ERIM International, Inc. and ISCIENCES, L.L.C. (October 1998).

[9] Miller, J. L., [*Principles of Infrared Technology: A Practical Guide to the State of the Art*], Van Nostrand Reinhold (1994).

[10] Welch, G. and Bishop, G., "An introduction to the kalman filter," tech. rep., University of North Carolina at Chapel Hill (1995).

[11] Lefebvre, E., ed., [*Advances and Challenges in Multisensor Data and Information Processing*], vol. 8 of *Sub-Series D: Information and Communication Security*, IOS Press (2007).

[12] Gan, Q. and Harris, C. J., "Comparison of two measurement fusion methods for kalman-filter-based multisensor data fusion," *IEEE Transaction on Aerospace and Electronics Systems* **37**, 273–280 (January 2001).

[13] Hall, D. L. and Llinas, J., "An introduction to multisensor data fusion," in [*Proceedings of the IEEE*], **85**, 6–23 (January 1997).

[14] Varshney, P. K., "Multisensor data fusion," *Electronics & Communication Engineering Journal* , 245–253 (December 1997).